Experimental study of collective acceleration of ions from a localized gas cloud

L. E. Floyd, W. W. Destler, and M. Reiser
Electrical Engineering Department and Department of Physics and Astronomy, University of Maryland, College Park, Maryland 20742

H. M. Shin
Seoul National University, Seoul, Korea

(Received 25 July 1980; accepted for publication 3 October 1980)

The collective acceleration of ions (H, D, He, N, Ne, Ar, Kr, Xe) to peak energies of about 5 MeV/nucleon has been achieved using a 1.5-MeV, 35-kA, 30-ns electron beam pulse. Ion energies have been measured using time-of-flight, range-energy/track etching, and nuclear diagnostics.

PACS numbers: 52.80.Vp, 52.60. + h, 52.90. + z

I. INTRODUCTION

In collective acceleration, the intense space-charge fields of electron clouds are used to accelerate ions. Apart from the interest in collective effects in general, the major motivation for the continuing work in the field is the fact that collectively produced electric fields have been observed to be about two orders of magnitude larger than fields than can be produced between electrodes. The use of intense relativistic electron beams (IREB) collectively to accelerate ions was first suggested theoretically by Veksler and Budker.[1] Devices based on that principle became practical after the development of high-current, relativistic electron beam generators in the middle 1960's. Initially, the use of magnetically trapped electron rings to accelerate ions appeared theoretically the most attractive scheme; however, subsequent experiments at several laboratories showed that electron rings have inherent instabilities that make their control much more difficult than originally supposed.[2] Much interest in the linear approach to collective acceleration began when Graybill and Uglum[3] found that hydrogen and nitrogen ions could be accelerated to peak energies of two or three times the electron beam energy when an electron beam was injected into a neutral gas column. In contrast, collective acceleration in vacuum is the acceleration of ions from a plasma localized in or near an IREB diode. Collective acceleration of protons in vacuum was first observed by Korop and Plyutto,[4] who were continuing similar work done earlier on plasma-filled diodes.[5] Luce[6] observed collective acceleration in an IREB diode with a dielectric or insulating anode, later named the Luce diode configuration. In this type of collective acceleration, a dielectric anode serves to provide a source of ions for the acceleration process. Protons of up to 20 times the electron beam energy, and also carbon and fluorine ions with energies of several MeV/amu have been observed in these systems. Further studies[7,8] have shown that downstream structures, such as lenses or a helix, could increase both the number and the energy of the ions. Collective acceleration in vacuum has also been observed from ion sources, such as electron bombardment of conducting anodes[9] and anode foils,[10] and laser-produced plasmas.[11] Many theories have been advanced to explain collective acceleration in the various experimental configurations.[2,11–14]

More recently, experiments were reported by our group at the University of Maryland using still another source of ions.[8,15] In these, a fast-rise gas-puff valve was used to provide a localized gas cloud downstream of the anode. The electron beam ionized and accelerated these ions of various species (H, He, N, Ne, Ar, Kr) to very high energies. In the initial studies, the accelerated ion energy was determined by the time-of-flight of the ion pulses between two charge-collection probes. It was found that the peak velocity of the accelerated ions was approximately 0.1 C, independent of the ion mass. This corresponds to a peak energy of about 4.7 MeV/amu in all cases. In this paper, we present experimental confirmation of these ion energies using two additional diagnostics, and report the acceleration of deuterium and xenon ions to comparable velocities. Section II details the experimental work, and conclusions are drawn in Sec. III.

II. EXPERIMENTS

The experimental configuration used is shown in Fig. 1. The electron beam generator consists of a Marx generator, Blumlein line, and a peaking switch that eliminates any beam precursor. Originally designed for electron ring generation, in the present configuration it delivers a 1.5-MV, 35-kA, 30-ns FWHM (full width at half maximum) negative pulse at the electron beam diode. The electron beam is field emitted from a 4-mm-diam cold tungsten cathode whose tip has been rounded to minimize mechanical damage. The stainless-steel anode, 5 mm downstream from the cathode, has a 20-mm hole on axis. The diode chamber is 25 cm in diameter. Faraday cup measurements downstream and magnetic pickup loops upstream show that within experimental error the electron beam propagates through the anode with little diminution.[11] This is corroborated by the fact that little or no damage is ever observed on the stainless-steel anode. Diode voltage and current are monitored using a capacitive voltage probe and current loop, respectively, both located at 18 cm upstream of the anode. The fast-rise puff valve is located in the downstream drift tube with its nozzle mounted on the anode about 1 cm from the anode hole. The valve is fired slightly in advance of the beam electrons, the delay varying from 425 to 700 μs, depending on the species of gas used. In general, the heavier the gas, the longer the delay

 0021-8979/81/020693-06$01.10

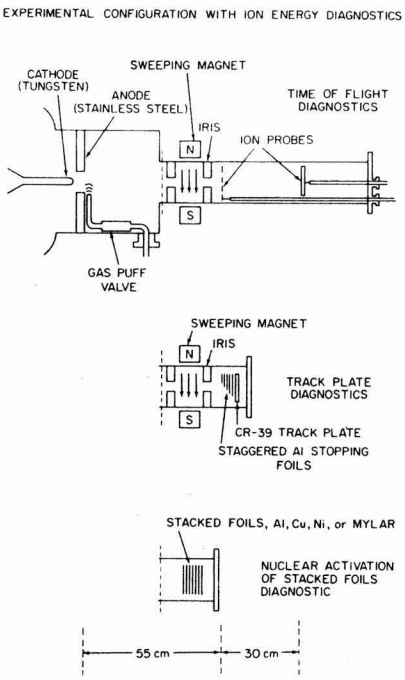

FIG. 1. General experimental configuration and ion energy diagonstics.

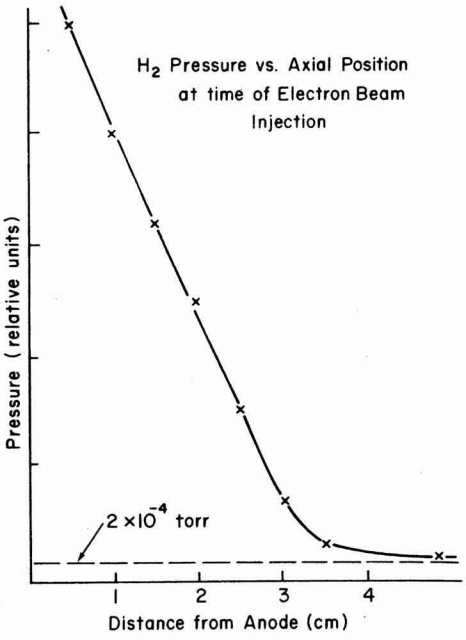

FIG. 2. Typical injected gas pressure at time of electron base injection vs axial position downstream of anode.

has to be for significant acceleration to take place. The optimum delay was found by trial and error. The performance of the puff valve was evaluated using a fast ionization guage whose approximate description may be found in Refs. 16 and 17. An example of the pressure profile at the time of injection is presented in Fig. 2. It should be observed that almost the entire gas cloud is located within 2 cm of the anode. A gate valve separates the diode chamber from the ion-energy diagnostics located downstream. The experiments described here were performed in a background vacuum of less than 1×10^{-4} Torr. Three different diagnostic methods were used to determine ion energies, the description and results of which are included in Secs. IIA, IIB, and IIC.

A. Time of flight

The time-of-flight (TOF) apparatus consists of a sweeping magnetic field, irises placed on each side of the magnetic field, and two intercepting current collector probes spaced 30 cm apart (Fig. 1). The sweeping magnetic field (1.5 kG for an axial distance of 5 cm) is used to block the beam electrons while leaving energetic ions relatively unaffected. The upstream and downstream irises have diameters of 3.3 and 2.5 cm, respectively. The upstream current probe, which has a circular screen 7.5 cm in diameter and is 62% transparent, is connected to the center conductor of a 50-Ω coaxial cable. The second probe, a solid brass disk 7.5 cm in diameter, is connected to an equal length of coaxial cable. Both cables are

TABLE I. Probe signal analysis.

Shot number	Species	t_0 (ns)	t_1 (ns)	t_2 (ns)	t_3 (ns)	τ_1 (ns)	τ_2 (ns)	I_p (A)	Q_i/Q_{He}	W_m (MeV)
2184	H	30	10	15	30	40	100	32	2.0	4.7
2439	D	...	10	15	35	60	170	5.0	0.64	9.4
2208	He	30	10	11	30	140	135	6.9	1.0	19.6
2192	N	28	10	15	35	150	140	5.9	0.9	65
2264	Ne	30	11	7	50	120	290	8.3	1.3	77
2187	Ar	29	10	15	70	150	245	6.9	1.1	186
2207	Kr	27	10	...	65	140	165	4.5	1.0	390
2452	Xe	...	8	15	...	130	>250	1.9	0.18	964

t_0 - time between peak of voltage and first rise.
t_1 - time between first rises of the two probes.
t_2 - time between first peaks.
t_3 - time between second peaks.
τ_1 - duration of first probe pulse.
τ_2 - duration of second probe pulse.

connected to different traces of a fast dual-beam oscilloscope. The simultaneity of the firing of both oscilloscope traces is checked on each shot by fiducial signals placed by a time-mark generator on each trace of the current collector probes, as well as on the electron beam generator voltage and current traces. A lower limit on the peak velocity of the ions may then be determined by dividing the distance between the probes by the time elapsed between the first rises of the current probe traces. With somewhat more ambiguity as to real particle energies, times between reproducible features on the two probes may also be used to compute velocities as well.

Typical TOF data obtained when the electron beam was fired through H, D, He, N, Ne, Ar, Kr, and Xe gas clouds, as well as probe signals with no gas injected, are displayed in Fig. 3. With the additions of D and Xe, these are the same results presented in our earlier letter.[15] The probe current traces for xenon on a magnified time scale are also included. For this case, the first rise of the two traces show a TOF of 8 ns between the two probes, implying a peak energy of 964 MeV. These data were selected from many samples taken under various experimental conditions. They represent, in the case of the heavy ions, the fastest observed ion velocity for each species. The general features of the current traces in the figure show that the beam front, containing the fastest ions, rises almost linearly to a first peak or plateau, which represents ions of an intermediate energy. This peak is then, in most cases, followed by a second peak representing a still lower-energy group of particles. The various travel times between the two probes associated with these features are described and summarized in Table I. Details on the analysis of the current traces may be found in the previous letter.[15]

The beam front velocity $v = 30\ \text{cm}/t_1$ represents a lower limit for the peak energy in the particle distribution. (For the identification of the various times, see Fig. 3.) It is observed that in all cases the velocity is within the range of $\beta = v/c = 0.10 \pm 0.02$, which is a remarkable result considering that the range of the mass of the ions studied is 1–131 amu. With regard to the velocities inferred from the current peaks, it is not at all clear that they are comprised of the same group of particles; thus, the velocities that one infers from t_2 and t_3 cannot be directly correlated with particle energies. The primary purpose for presenting these numbers is to indicate the gross features of the observed ion pulses and the fact that a large portion of the ion beam has considerably less energy than the particles of the beamfront. To the extent that the TOF between the current peaks can be related to real particle velocities, the data show that the ratio of the number of high-energy ions to low-energy ions decreases with increasing ion mass. With the exception of D and Xe, the amount of charge collected was found to be approximately constant for all ions. The fact that data for those species are somewhat different than for the other gases should not be considered critical, since this data was taken after many small changes in the experimental configuration had taken place. In any case, the values for total charge collected and peak current have errors of unknown size due to secondary electron emission from ion impact with the probes. The charge states of the accelerated ions are unknown; however, the presumption is made that, unless the ions are very highly

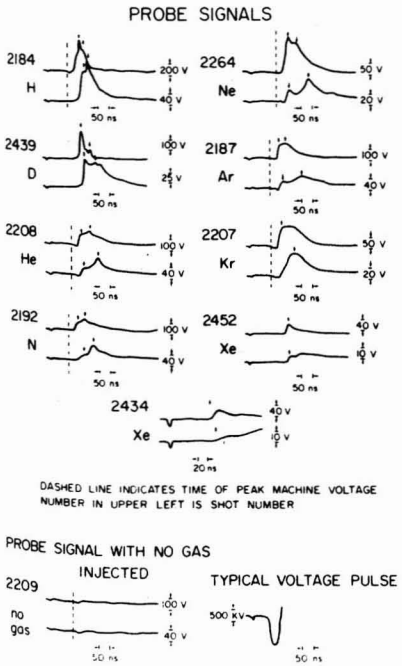

FIG. 3. Time-of-flight ion current waveforms for various injected gas species. Probe separation is 30 cm.

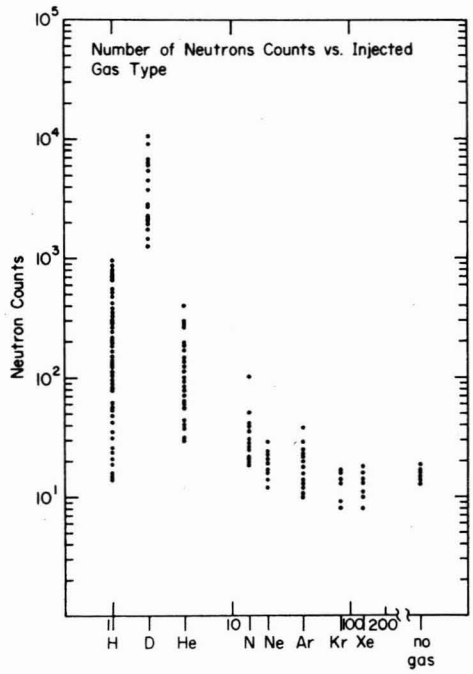

FIG. 4. Neutron counts/100 s for various injected gases. Background is typically 10–20 counts/100 s.

TABLE II. Maximum energy obtained using stacked foil nuclear activation diagnostics.

Gas	Foil type	Reaction observed	Energy threshold used (MeV)	Foil thickness (mil)	Number of foils activated	Inferred energy (MeV)	Inferred velocity (β)
H	Copper	$Cu^{63}(p,n)Zn^{63}$	4.21	2	7	6.3 (14)[a]	0.12
D	Mylar	$C^{12}(d,n)N^{13}$	0.7	1	13	7.9	0.092
He	Nickel	$Ni^{60}(\alpha,n)Zn^{63}$	13	0.2	6	18	0.098
N	Aluminum	$Al^{27}(N^{14},N^{13})Al^{28}$	40	0.65	1[b]	40	0.078

[a]The number in parentheses is an early result obtained with a 2-mm cathode, a smaller anode hole, and a different gas distribution.
[b]Attempts to activate more than one aluminum foil have not yet been attempted.

stripped, it is unlikely that they could be accelerated to such high energies. If this assumption is made, the approximate constancy of the charge collected implies that the number of particles detected becomes smaller with increasing ion mass.

The TOF system was also operated without the sweeping magnet. In this configuration, negative signals typically ten or greater times in magnitude than the ion signal are observed to arrive at the same time as the ions. This indicates that a strong coupling exists between the electron and ion motion, which results in a beam front propagation velocity for both of $v = 0.1$ C.

B. Nuclear diagnostics

The energies of light ions, such as hydrogen and helium, accelerated in our laboratory have also been detected using nuclear activation of stacked foils. The energy of an ion activating the nth foil of the stack may be inferred to be the sum of the threshold energy for nuclear reaction and the energy found by integration of the stopping power through $(n-1)$ foils, the information for which is readily obtained from the literature.[18] The investigation of the acceleration of heavy ions either from gaseous or laser ion sources has diagnostic complications in comparison to light ions in that nuclear activation cross sections become smaller and their corresponding threshold activation energies become much larger due to the increasing Coulomb energy barrier. The graph in Fig. 4 delineates the domain of applicability of nuclear reactions through the observation of energetic ion-induced neutron-producing reactions. Displayed is the number of neutron counts observed after collective acceleration shots using a silver activation neutron detector with respect to ion type. The data included here were obtained under various experimental conditions, both with and without suitable target material for the ions accelerated. The general trend of lower neutron counts at higher atomic mass numbers supports the contention that nuclear diagnostics become progressively less effective for heavy ions at the energies that are produced.

Nuclear foil activation was performed by the placement of a target foil stack immediately downstream of the gate valve facilitating its convenient removal (Fig. 1). Reactions included in this analysis were $Cu^{63}(p,n)Zn^{63}$,[7] $C^{12}(d,n)N^{13}$,[7] $Ni^{60}(\alpha,n)Zn^{63}$,[19] $Al^{27}(N^{14},N^{13})Al^{28}$,[20] and $Al^{27}(N^{14},\alpha,3n)Cl^{34m}$ (Ref. 20) for gases H, D, He, and N, respectively. As stated previously, nuclear diagnostics were not productive with ions heavier than nitrogen. The data, summarized in Table II, represent the highest energies obtained for each ion type under varying experimental conditions. The relevant isotopes were identified by their γ spectra and half-lives. The general trend of higher energies with larger atomic masses should be noted.

In another experiment, a Faraday cup was placed 31 cm downstream of the diode to collect electron current. Using hydrogen gas, many shots were fired at various gas cloud densities. Plotted in Fig. 5(a) are the currents received at the Faraday cup versus injected gas pressure, and in Fig. 5(b) are plotted the neutron counts observed in each case. Neutron production has been found to be a good measure of the effectiveness of proton acceleration in these systems. Comparison of the two graphs shows clearly that optimum neutron production, and thus optimum acceleration, takes place when enough ions are present to allow electron beam propagation.

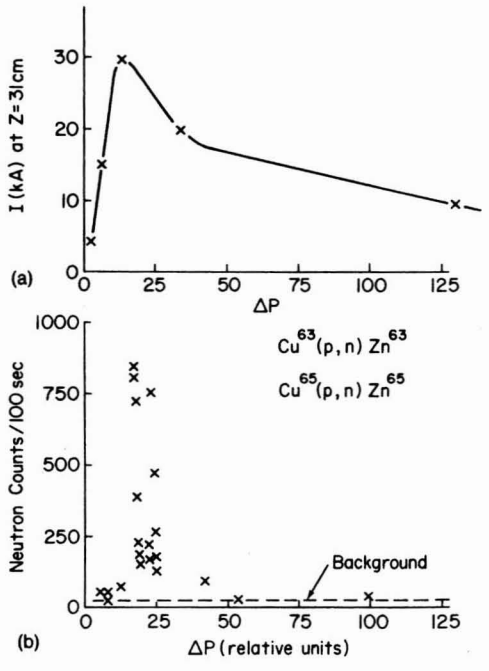

FIG. 5. (a) Current reaching z-31 cm downstream of the anode vs injected hydrogen gas pressure. (b) Neutron counts/100 s vs injected gas pressure.

TABLE III. Maximum energy of ions from track plate diagnostics.

Gas	Maximum penetration thickness in Al (mil)	Peak energy (MeV)	Energy/nucleon (MeV)
H	18	8.3	8.3
D	7.15	6.5	3.2
He	10	23.6	5.9
N	6.5	127	9.1
Ne	4.55	170	8.5
Ar	2.6	250	6.2
Kr	1.3	276	3.3
Xe	1.95	638	4.9

C. Range-energy/track etching

The third energy diagnostic is the etching of track plates shielded by foils of known stopping power. The substrate used for track etching was a transparent material CR-39 (modified polycarbonate), a material found by us to be more sensitive to energetic ions than diacel cellulose nitrate. The material of known stopping power was chosen to be aluminum foil available in 0.65- and 1-mil thicknesses. The foils were staggered in thicknesses of as many as 15 or 20 foils and taped directly to the track plate. The track plate was then positioned at the same location as the front TOF probe (Fig. 1). Once exposed, the track plate with foils removed was immersed in a 6.25-N NaOH bath at 70 °C for two hours. The particle tracks, only individually visible under a microscope, are perceived with the naked eye as a frosting on the CR-39 surface. The stopping-power tables used for analyzing this data were that of Northcliffe and Schilling.[18]

The etching of tracks shielded by stacked aluminum foils was performed with the same gases as were used with the TOF experiments. The number of foils penetrated and their corresponding inferred peak energy for each ion type is given in Table III. The values listed for the number of foils penetrated are those in which the tracks present are in sufficient number to make the identification conservative and unambiguous. By counting the number of tracks after a given foil, an estimate of the number of ions above a certain energy may be obtained. In the case of xenon, about 10^7 ions were observed at energies above 638 MeV.

III. CONCLUSIONS

The results of the three different ion energy diagnostics are summarized in Fig. 6 and the plot shows clearly the good general agreement between the measurement techniques. We have concluded that the ions observed are the same species as the gas-injected for the following reasons: (1) no ions are observed on the TOF probes when no gas is injected; (2) although tracks are observed on plates that are not shielded by aluminum foil when no gas is injected, no tracks whatsoever were observed underneath even one foil (if these were hydrogen ions, their energy would be less than 1.1 MeV; (3) as mentioned earlier, nuclear diagnostics have verified the acceleration of H, D, He, and N to energies comparable to those found by track etching and TOF; (4) neutron counts above background are not observed on heavy gas shots indicating that light ions are not present in significant quantities under those conditions; (5) the timing between the firing of the puff valve and the electron beam generator was found experimentally to be critical if high-energy ions are to be observed at all, thus showing the importance of the presence of the gas to the acceleration mechanizm; (6) the track data show that the accelerated ions penetrate through progressively fewer stopping foils as the mass of the injected gas atoms increases, which is consistent with known stopping data; (7) the energies obtained with the track plates and the TOF are in approximate agreement for all masses. We therefore conclude that electron beam injection into a localized gas cloud has led to the collective acceleration of ions to peak velocities of approximately 0.1 C regardless of ion mass.

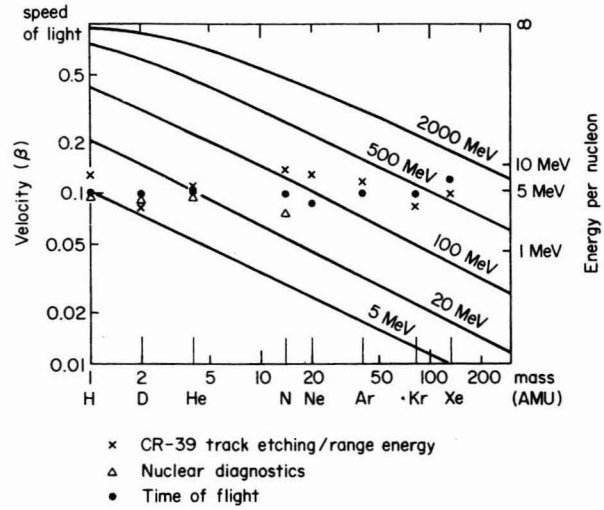

FIG. 6. Ion velocity (and energy) as a function of the mass of the injected gas measured by three different diagnostic techniques.

In summary, the major conclusions to be drawn from these studies are as follows.

(1) H, D, He, N, Ne, Ar, Kr, and Xe ions have been accelerated to peak energies of about 4.7 MeV/amu using a 1.5-MeV, 35-kA, 30-ns FWHM electron beam pulse.

(2) About 10^7 Xe ions/pulse have been accelerated to energies above 638 MeV.

(3) There is no evidence that impurity ions from the background vacuum or from the anode and cathode surfaces are accelerated in any significant numbers or to any significant energies.

(4) The relatively small number of the highest-energy ions are accompanied by larger numbers of intermediate energy (1–4 MeV/amu) ions.

(5) The use of the conducting-anode/puff-valve system in place of the dielectric anode in Luce-type systems allows independent control of the number and species of the ions to be accelerated.

ACKNOWLEDGMENTS

Experimental and technical assistance were provided by J. A. Pyle, D. N. Cohen, and C. J. Shedlock. The authors acknowledge valuable discussions with M. J. Rhee and S. E.

Graybill. The idea to use CR-39 for track etching is due to W. Bostick. This research was supported by the National Science Foundation and the Air Force Office of Scientific Research. This paper is from a dissertation to be submitted to the Graduate School, University of Maryland, by Linton Floyd in partial fulfillment of the requirement for the Ph.D. degree in Physics.

[1]V. I. Veksler, in Proceedings of CERN Symposium on High Energy Accelerators, Geneva, 1956 (unpublished); G. I. Budker, *ibid.*; At. Energy Aust. **1**, 9 (1956).
[2]C. L. Olson and U. Schumacher, in *Springer Tracts in Modern Physics: Collective Ion Acceleration*, edited by G. Hohler (Springer, New York, 1979), Vol. 84.
[3]S. Graybill and J. Uglum, J. Appl. Phys. **41**, 236 (1970).
[4]E. D. Korop and A. A. Plyutto, Zh. Tekh. Fiz. **41**, 1055 (1971) [Sov. Phys. Tech. Phys. **16**, 830 (1971)].
[5]A. A. Plyutto, Sov. Phys. JETP **12**, 1106 (1961).
[6]J. S. Luce, Ann. N. Y. Acad. Sci. **20**, 336 (1973).
[7]J. S. Luce, Ann. N. Y. Acad. Sci. **251**, 217 (1975).
[8]W. W. Destler, L. Floyd, and M. Reiser, IEEE Trans. Nucl. Sci. **26**, 4177 (1979).
[9]S. Takeda, M. Tamura, T. Yamamoto, and M. Kawanishi, Jpn. J. Appl. Phys. **18**, 641 (1979).
[10]P. L. Taylor, J. Appl. Phys. **51**, 22 (1980).
[11]W. W. Destler, H. S. Uhm, H. Kim, and M. Reiser, J. Appl. Phys. **50**, 3015 (1979).
[12]J. W. Poukey and N. Rostoker, Plasma Phys. **13**, 897 (1971).
[13]L. S. Bogdankevich, I. L. Zhelyazkov, and A. A. Rukhadze, Sov. Phys. JETP **30**, 174 (1970).
[14]L. S. Bogdankevich and A. A. Rukhadze, Sov. Phys. Usp. **14**, 163 (1971).
[15]W. W. Destler, L. E. Floyd, and M. Reiser, Phys. Rev. Lett. **44**, 70 (1980).
[16]E. A. Valsamakos, Rev. Sci. Instrum. **37**, 1318 (1966).
[17]G. J. Schulz and A. V. Phelps, Rev. Sci. Instrum. **28**, 1051 (1957).
[18]L. C. Northcliffe and R. F. Schilling, Nuclear Data Tables **7A**, 233–463 (1970).
[19]I. Kaplan, in *Nuclear Physics*, 2nd edition (Addison-Wesley, Reading, Mass. 1963), p. 483.
[20]I. M. Ladenbauer-Bellis, I. L. Preiss, and C. E. Anderson, Phys. Rev. **125**, 606 (1962).